An Unsupervised Urban Change Detection Procedure by Using Luminance and Saturation for Multispectral Remotely Sensed Images

Su Ye and Dongmei Chen

Abstract

Unsupervised change detection techniques have been widely employed in the remote-sensing area when suitable reference data is not available. Image (or Index) differencing is one of the most commonly used methods due to its simplicity. However, past applications of image differencing were often inefficient in separating real change and noise due to the lack of steps for feature selection and integration of contextual information. To address these issues, we propose a novel unsupervised procedure which uses two complementary features, namely luminance and saturation, extracted from multispectral images, and combines T-point thresholding, Bayes fusion, and Markov Random Fields. Through a case study, the performance of our proposed procedure was compared with other three unsupervised change-detection methods including Principle Component Analysis (PCA), Fuzzy c-means (FCM), and Expectation Maximum-Markov Random Field (EM-MRF). The change detection results from our proposed method are more compact with less noise than those from other methods over urban areas. The quantitative accuracy assessment indicates that the overall accuracy and Kappa statistic of our proposed procedure are 95.1 percent and 83.3 percent, respectively, which are significantly higher than the other three unsupervised change detection methods.

Introduction

There is a growing interest in monitoring land-use/land-cover change as it provides up-to-date information for many applications. Employing remote-sensing (RS) technology has been critical for keeping track of land-use/land-cover transition at a variety of spatial scales (Rogan and Chen, 2004; Hussain *et al.*, 2013). Compared with traditional monitoring methods (such as field surveying), RS-based change detection can better allow for processing large areas, producing quantitative results and offering repeatable procedures (Coppin *et al.*, 2004).

Numerous state-of-the-art approaches have been developed to analyze RS imagery for change detection. These methods are usually categorized into supervised and unsupervised methods, according to the availability of adequate reference data (Bruzzone and Prieto, 2000; Bruzzone and Prieto, 2002; Fernandez-Prieto and Marconcini, 2011). The advantage of supervised change detection is the capability of labeling the type of change (the detailed "from-to" information) based on given training samples. However, the generation of suitable multi-temporal reference data to characterize all the classes is usually a difficult task, especially for historical images (Lu *et al.*, 2004). Compared with supervised methods, unsupervised ones can be much more cost-effective since no reference data is required. In spite of being unable to offer the information on categories of land transition, the changed/no-change detection is often acceptable for many practical applications (Hussain *et al.*, 2013).
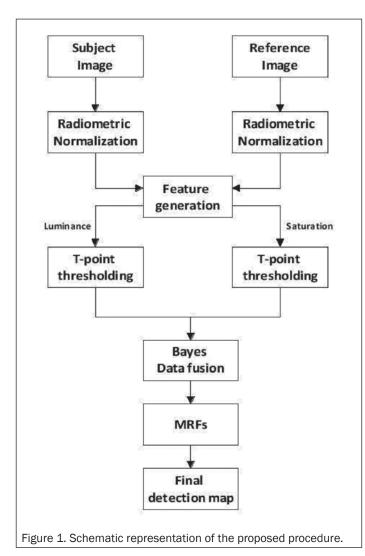
Image differencing (or index differencing) is one of the most commonly used methods for unsupervised change detection (Bruzzone and Prieto, 2002; Rogerson, 2002; Lu *et al.*, 2004). Compared with other unsupervised approaches, such as Principle Component Analysis (Deng *et al.*, 2008) or clustering algorithms (Bruzzone and Prieto, 2000), image differencing is much cheaper computationally, and it is easier to interpret its results (Lu *et al.*, 2004; Hussain *et al.*, 2013). The basic idea for image differencing stems from the fact that the physical status of land area can be characterized by certain feature indices derived from the remotely sensed data; when we analyze targeted features from bi-temporal images, the larger its deviating values from means of unchanged class appear to be, the more likely it is that change has occurred in the corresponding area. The useful features for image differencing can be defined as digital number in a single spectral band, vegetation indexes (Singh, 1989), principle component (Deng *et al.*, 2008), or texture index (Tomowski *et al.*, 2010). Feature-differencing values of interested areas are usually passed to a thresholding strategy to separate "no-change" and "changed" class for the final result map.

However, image or index differencing often exhibits inconsistent performances, as it makes its decision relying only on single feature analysis. For most urban change-detection tasks, when single feature differencing is applied, we may have (a) real change information corresponding to transition between different land-cover types which are usually of interest, and (b) noisy change identification due to other factors, such as seasonal growth or local illumination variance. In the complicated practical scenes, clusters of real and noisy changes are sometimes mixed together in the feature space; thus, we are unable to completely separate them by using a single thresholding value. In this sense, fusion techniques merging multiple difference images have been introduced to improve detection accuracy (Le Hégarat-Mascle and Seltz, 2004; Du *et al.*, 2012), since different features might offer complementary information about the patterns to be classified (Kittler *et al.*, 1998) .

The second issue with traditional image differencing is that global analysis of difference image fails to account for local spatial information influencing the reliability of final result. To address this issue, one solution is incorporating the direct difference of certain texture indices for change detection (Li and Leung, 2002; Tomowski *et al.*, 2010). Another method is applying Markov Random Fields (MRFs) models (Bruzzone and Prieto, 2000; Kasetkasem and Varshney, 2002; Zhang *et al.*, 2007; Benedek and Szirányi, 2009), which has

Department of Geography, Queen's University, Kingston, Ontario, K7L 3N6 (chendm@queensu.ca).

Figure 1. Schematic representation of the proposed procedure.

experimentally demonstrated its advantages in exploiting the spatial-contextual information contained in the difference image because of its well-established mathematical foundation. These models assume that the feature value at each pixel relies on the values of only its neighboring pixels, and can simultaneously ensure the consistency of the class labels with local extent and spatial smoothness through interaction between neighboring pixels (Benedek and Szirányi, 2009).

Based on the aforementioned remarks, we propose a novel methodology for unsupervised change-detection methodology relying on the combination of multiple features. The general scheme of proposed method consisted of five steps:

1. automatic radiometric normalization for preprocessing;
2. two relatively independent feature extraction, i.e., luminance and saturation, are chosen to perform the specific urban change-detection work;
3. the T-point algorithm is conducted to get reasonable thresholding values for each feature image;
4. Naïve Bayes is then adopted to combine two feature classification results based on the probability density function for each class; and
5. as the last step, MRFs framework is responsible for integrating spatial-contextual information and generating the final map.

This paper is organized into four parts. In the second section, we mainly address the detailed description of the steps involved in our proposed procedure. In the section on experimental result, the outcomes of exploring single feature are presented to show their relationship first; both qualitative and quantitative comparison between our method and other three previous unsupervised approaches are presented after; the final section discusses our work, and a conclusion is presented.

Proposed Method
The overall schema for the proposed procedure is given in Figure 1. Each component is described in detail in the following.

Radiometric Normalization
Reflectance properties of pixels are affected by various illumination or atmospheric effects, requiring radiometric normalization (RN) before pixel-by-pixel comparison. The method of Pseudo-Invariant Feature (PIF) (Sohl, 1999; Im and Jensen, 2005) has been commonly used for RN in the previous research, which builds a regression relationship of two scenes based on the "no-change" pixels from manual sampling. However, from our point of view, the manual selection of Pseudo-Invariant pixels goes against the principle of unsupervised techniques. In this paper, a two-fold regression procedure is introduced to automatically accomplish relative radiometric normalization: first we apply Image Regression (IR) (Yang and Lo, 2000) to estimate the linear regression relationship on the pixels of whole image, and get the initial difference image; then we implement T-point thresholding to separate the unchanged set from the differencing image obtained by the first regression, and finally we derive the final linear regression equation based on the unchanged pixels after thresholding.

HSL Color Space and Feature Generation
HSL (or HSI, HSV) color representation, an alternate to others (e.g., RGB color model), is considered more intuitive to human perception than others, and has been applied for many previous image processing tasks (Zhang and Wang, 2000; Hu *et al.*, 2005; Dhandra *et al.*, 2006). More importantly, using such color representation can effectively reduce inter-band correlation (Gillespie *et al.*, 1986; Lei, 1999) through separating three relatively independent parts: luminance, hue, and saturation.

Luminance ("L") is the brightness descriptor, which is utilized to represent the total amount of lightness. Hue (H) and saturation (S) jointly describe the color of an image: "H" represents the dominant wavelength in the spectral distribution; "S" represents a measure of the purity of the color (Dhandra *et al.*, 2006). Hue value is often very unstable when the saturation is low (Cheng *et al.*, 2001; Dhandra *et al.*, 2006), probably leading to numerous errors with any type of thresholding strategy because of the inconsistent shape of the histogram. Accordingly, only saturation is selected in our method to represent color information.

There are two other similar methods of generating color features for options, (hue-saturation-intensity (HSI) and hue-saturation-value (HSV) color models. HSI is considered to have the highest correlation, because its saturation is defined without being standardized; the difference between HSL and HSV is that a decrease in HSL in saturation results in a loss of color strength while maintaining the same visual brightness; whereas in HSV a reduction in saturation causes the visual brightness to increase. From our point of view, HSL is more suitable than HSV for the proposed modal because there is less correlation between the components, since a good independence level among features is the basic assumption for the subsequent Bayes fusion.

Image Differencing and Thresholding
Direct pixel-by pixel differencing result is implemented in our procedure instead of traditional absolute differencing (Bruzzone and Prieto, 2000; Le Hégarat-Mascle and Seltz, 2004), in case of the issue of asymmetrical change occurring
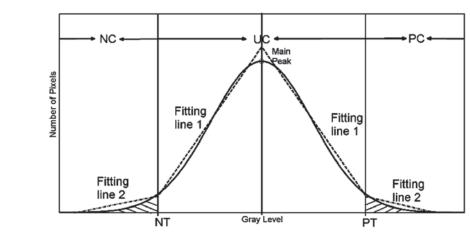
Figure 2. Illustration of two-sided T-point algorithm applied in the proposed technique.

in many practical scenes. Differencing values can be negative or positive, producing two tails in the histogram (Figure 2). We divide the histogram curve of difference image into left and right side by highest peak of histogram. For each side, the T-point algorithm (Coudray *et al.*, 2010) was used to determine the change threshold. The T-point algorithm, developed specifically for unimodal histogram through finding the best fitting lines for each part, has been proved to be more effective for urban areas based on our previous tests (Chen *et al.*, 2014). It is easy to find two decision boundary, i.e., one negative threshold (NT) and one positive threshold (PT), separating the feature space into three classes: negative change (NC), positive change (PC) and unchanged class (UC).

Bayes Fusion

Data fusion is applied in order to fuse the two class maps corresponding to luminance and saturation features after applying the two-sided T-point algorithm. Generally, there are two common types for fusing two independent data band: the first type is based on the crisp output produced by each dataset, such as majority voting or "and/or" operation; the second type produces the fuzzy output for each band first, and then combine them following some rules, which is often viewed as a better way to handle uncertainty and imprecision (Grant *et al.*, 2008). The Bayes fusion in our proposed method belongs to the second type.

For Bayes fusion, there are nine possible cases l_k for the joint labels (*L*) based on three change results (negative change ω_{nc}, positive change ω_{pc} and no change ω_{uc}) for each feature. Let a vector $x = (x_{lu}, x_{sa})$ denote the signature of a pixel, where x_{lu} is its luminance value, and x_{sa} is its saturation value. Since the luminance and saturation bands are approximately independent as the property of HSL color space, according to Naïve Bayes fusion theory (Kuncheva, 2004), the expression for the combined probability that L will take on $x(x_{lu}, x_{sa})$ can be written as:

$$p(L=l_k \mid x) \propto p(x_{lu} \mid L=l_k)p(x_{sa} \mid L=l_k)*p(L=l_k) \qquad (1)$$

where $p(x_{lu} \mid L=l_k)$ and $p(x_{sa} \mid L=l_k)$ are posterior probability conditioned on the combined class l_k, $p(L=l_k)$ is the *priori* probability function based on occurrence of l_k. As luminance and saturation are independent with each other, Equation 1 can be written as:

$$p(L=l_k \mid x) \propto p(L=l_k)*p(x_{lu} \mid \omega_i(lu))p(x_{sa} \mid \omega_i(sa)) \qquad (1)$$

where $p(x_{lu} \mid \omega_i(lu))$ and $p(x_{sa} \mid \omega_i(sa))$ are posterior probability given on the class based on each separated feature. The final

change-detection result of pixel is assigned to the class that maximizes the discriminant function (Equation 2). For posterior probability, we can model it by defining the probability density functions (PDFs) for each class; for the component of prior probability and the combined probability for both posterior and prior probability, a Markov-based approach will be applied to give optimal estimations. These two components are discussed respectively in the following two subsections.

Modeling Probability Density Functions (PDFs)

It is usually easy to define the PDFs of "no-change" class (by using normal distribution with $\mu=0$ since we have normalized every original band), while modeling "change" class provides a challenging task as the nature of the changes is unknown. To define normalized PDFs for each class, we follow the previous work done by Le Hégarat-Mascle and Seltz (2004) and make some modifications for our two-sided thresholding scene. Several properties should be met for our specific application:

1. When the absolute values of feature index values increases, $p(x \mid \omega_{nc})$ and $p(x \mid \omega_{pc})$ increases, $p(x \mid \omega_{uc})$ decreases;
2. The highest probability density for a class, $p(x=x_{min} \mid \omega_{nc})$, $p(x=x_{max} \mid \omega_{pc})$ and $p(x=0 \mid \omega_{uc})$ should be equal to 1 after normalization, where x_{min} is the x value of the first non-zero point in the histogram of difference image, x_{max} is that of the last non-zero point;
3. $p(x=NT \mid \omega_{nc})$ and $p(x=NT \mid \omega_{uc})$, $p(x=PT \mid \omega_{pc})$ and $p(x=PT \mid \omega_{uc})$ should be equal to each other, guaranteeing the probabilities of dominated class in its own region are larger than those in other classes, where is the negative threshold, is the positive threshold.

The distribution of ω_{uc} can be given by (Le Hégarat-Mascle & Seltz, 2004):

$$p(x \mid \omega_{uc}) = \exp\{\frac{-y^2}{2\hat{\sigma}_{uc}^2}\} \qquad (3)$$

where $\hat{\sigma}_{uc}$ can be obtained by estimating the standard deviation of all the pixels in the unchanged class. For the probability of density of ω_{pc} and ω_{nc}, we used a normalized sigmoid for each, which has the advantage of being an increasing function (Le Hégarat-Mascle & Seltz, 2004).

Markov Random Fields Framework

Markov Random Fields (MRFs) assumes that the prior probability of each pixel is uniquely determined by its local conditional probabilities. We define the neighbor system of the pixel *x* with coordinates (*s,t*) as a first-order spatial neighborhood $N(s,t)=\{(\pm1, 0),(0, \pm1)\}$. The prior probability for pixel
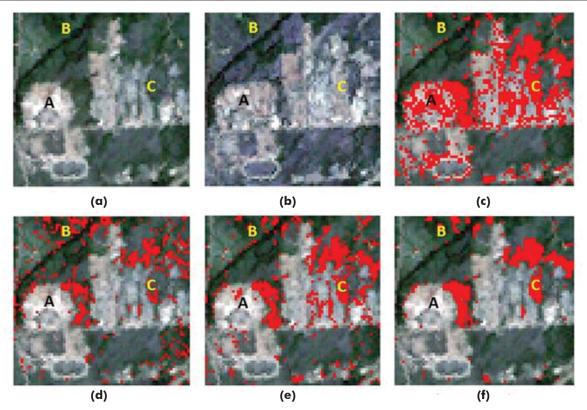
Plate 1. Examples of detection results for a small subset from steps in the proposed procedure: (a) the subset image acquired in 1991, (b) the subset images acquired and 2001, (c) the detection result from thresholding the luminance band, (d) the detection result from thresholding the saturation band, (e) the detection result after Bayes fusion of thresholding results in (c) and (d), and (f) the detection result after MRF smoothing the results in (e). Changed pixels are highlighted as red.

$x(s,t)$ belonging to a certain class l_i is only dependent on its neighborhood $N(s,t)$, and can be calculated as:

$$p\left(L_{(s,t)} = l_i\right) = p\left(L_{(s,t)} = l_i \mid L_{N(s,t)}\right) = \frac{1}{Z} \exp(-U\left(L_{(s,t)} = l_i \mid L_{N(s,t)}\right)) \quad (4)$$

where $U(L_{(s,t)}=l_i \mid L_{N(s,t)})$ is the Gibbs energy function for priori probability at the pixel (s,t), and Z is a normalizing factor $Z = 1/\sum_{l_i \in L_{(s,t)}} p(L_{(s,t)} = l_i)$. $U(L_{(s,t)} = l_i \mid L_{N(s,t)})$ can be characterized by the agreement in class labels between each pixel and its spatial neighbor by Kronecker delta function (Bruzzone and Prieto, 2000). The optimal label can be obtained when the sum of energy function of *priori* and posterior probability components over the all the pixels reaches the minimum. We apply a widely-used optimization algorithm, Iterative Conditional Modes (ICM) (Bruzzone and Prieto, 2000; Zhang *et al.*, 2007; Li *et al.*, 2011), to minimize the energy term.

Final Map Generation
As the result, we can get a nine-class classification result after MRFs modeling. There is no reference data to further confirm the detailed changed type ("from-to" information) for these nine subclasses. However, based on the assumption that only the overlap of luminance and saturation change can be the change that we are interested in, an unsupervised grouping strategy (Table 1) is used to get the final "change/no-change" results.

Experiments and Results

Study Data and Area
Our study area covers the main part of the City of Kingston located in Eastern Ontario, Canada where the St. Lawrence River flows out of Lake Ontario. The data consisted of two co-registered bi-temporal images and were respectively acquired by the Landsat-5 Thematic Mapper (TM) sensor in August 1990 and the Landsat-7 Enhanced Thematic Mapper Plus (ETM+) sensor in August 2001 (Plate 2a and 2b). With about 120,000 urban population, the study area has both urban and rural land-cover types. The urban area is located in the southern part of the study area adjacent to Lake Ontario. The northern part of the study area is mainly composed of agriculture land along with open space and forest. The dominated land-cover types include "built-up area," "grass," "forest," and "water." From 1990 to 2001, the City of Kingston has experienced a moderate growth of urban land expansion and vegetation change, making it an ideal case for testing the effectiveness of the proposed procedure for urban change detection.

Exploring Luminance and Saturation Bands for Urban Land-Cover Change Detection
The key technique for the proposed procedure is the feature selection. The ideal feature groups should have perfect complementary attributes that can exclude "noisy changes," while remaining most of real changes that we are interested in. Most urban change detection only focuses on the change
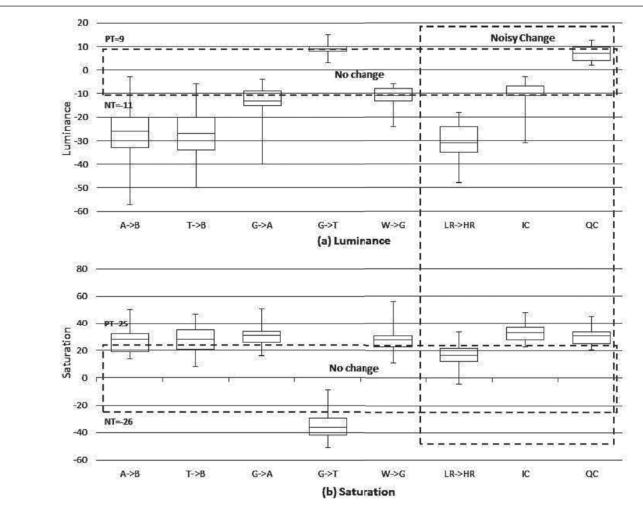
TABLE 1. GROUPING STRATEGY FOR FINAL CHANGE-DETECTION MAP BASED ON THE PRIOR ASSUMPTION THAT THE CHANGE ONLY OCCURS WHEN BOTH SATURATION AND LUMINANCE CHANGE

Subclass Names	
"Change class":	$l_1(\omega_{pc}(lu), \omega_{pc}(sa))$, $l_2(\omega_{nc}(lu), \omega_{pc}(sa))$, $l_3(\omega_{pc}(lu), \omega_{nc}(sa))$, $l_4(\omega_{nc}(lu), \omega_{nc}(sa))$
"No-change class":	$l_5(\omega_{uc}(lu), \omega_{pc}(sa))$, $l_6(\omega_{uc}(lu), \omega_{nc}(sa))$, $l_7(\omega_{pc}(lu), \omega_{uc}(sa))$, $l_8(\omega_{nc}(lu), \omega_{uc}(sa))$, $l_7(\omega_{uc}(lu), \omega_{uc}(sa))$

Figure 3. Box plots of feature [(a) luminance, and (b) saturation] statistics from sampled pixels, which consisted (1) 62 pixels from *Barren land* to *Built-up area* (A->B); (2) 33 pixels of *Trees* to *Built-up area* (T->B); (3) 57 pixels of *Grass land* to *Barren land* (G->A); (4) 55 pixels of *Grass land* to *Trees* (G->T); (5) 64 pixels of *Water* to *Grass land* (W->G); (6) 35 pixels of *low reflectance* to *high reflectance* (LR->HR); (7) 32 pixels of inter-class change of vegetation (IC); (8) 32 pixels of water quality change (QC). Positive Threshold (PT) and Negative Threshold (NT) were obtained by the T-point algorithm.

in land-cover types. They can be viewed as "real change" in this specific practical scene; change within one land-cover class is considered to be "noisy change" in our experiment.

Plate 1 shows single feature thresholding results after T-point algorithm and their fusion results for a small subset of the study area. The luminance image (Plate 1c) can detect most of the conversion between built-up area and other land-cover types. However, it over-detects some unchanged built-up area such as the region of 'A' in Plate 1c. Similarly, for saturation thresholding results (Plate 1d), there are some false detections such as the 'B' region, which are actually inter-class vegetation changes. In addition, the saturation thresholding result alone is likely to miss some important changes between built-up area and vegetation (such as 'C' region in Plate 1d). Plate 1e shows that the use of the strategy of Naïve Bayes for fusion can redetect some missed changes (such as 'C' region) and exclude false changes (such as 'A' region and 'B' region). For the last step, MRFs procedure allows detected objects to be more compact, and increases reliability of detection (Plate 1f).

Figure 3 is a box plot based on manual samples from different change of interest and noisy changes, to quantitatively confirm that luminance and saturation are complementary. There are five land cover types in our area of change: *Built-up*

Area (*B*), *Trees* (*T*), *Grass land* (*G*), *Barren land* (*A*), and *Water* (*W*). Our change of interest is the transition between any two of these five classes, such as from *Tree* to *Built-up Area* (*T->B*). We selected five representative change types of interest in our study region for making box plot: *A->B*, *T->B*, *G->A*, *G->T*, *W->G*. For noisy change in our study area, we think they are mainly caused by local different reflectance (*low reflectance* to *high reflectance*, *LR->HR*), quality change of water (*QC*), or inter-class changes of vegetation (*IC*).

For every type of change, a certain number of sampling pixels are collected according to visual interpretation. The statistics of sampling change classes on each feature band are shown together in the box plot; the positive (PT) and negative threshold (NT) obtained by T-point algorithm are given to show their relationship with those change classes. The boxplot indicates that luminance thresholding is good at identifying the noisy change *IC* and *QC* because more than 75 percent of them fall within the "No-change" region; saturation thresholding performs well in *LR->HR*; all the change types have at least 50 percent accurate detection rates for both two features. This result exhibits the potential of separating change of interest from all the changes by fusing the changed parts of luminance and saturation.
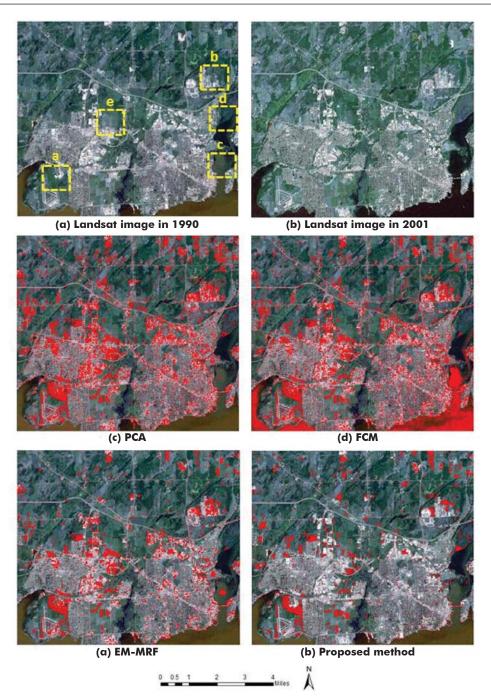
Plate 2. The multi-temporal Landsat TM images [(a) and (b)] and the change detection results from the different unsupervised change-detection approaches (c to f). The changed pixels are shown in Red. The five yellow dashed rectangles in (a) are the sub-areas that are illustrated in Figure 4.

Evaluation

The goal in this section is to quantitatively and qualitatively present comparative analysis of the proposed procedure with the other three common unsupervised change-detection methods from the literature, including two context-insensitive techniques (namely PCA and FCM) and one context-sensitive technique (namely EM-MRF).

1. Principle Component Analysis (PCA)

   Principle Component Analysis is based on transformation of the multivariate data to several uncorrelated bands. First, we merged the first three bands of two Landsat images into six bands and then applied PC

transform (Deng *et al.*, 2008). The changed information is usually considered to be in the second component. Since the histogram distribution of second band presents a unimodal pattern, two-sided T-point thresholding is used for separating changed and unchanged region.

2. Fuzzy c-means (FCM)

   Clustering is one of most common unsupervised techniques for image classification. A powerful technique from clustering family called fuzzy c-means has been adopted for unsupervised change detection (Ghosh *et al.*, 2009). This method is often considered to be more suitable than hard-membership approach for handling
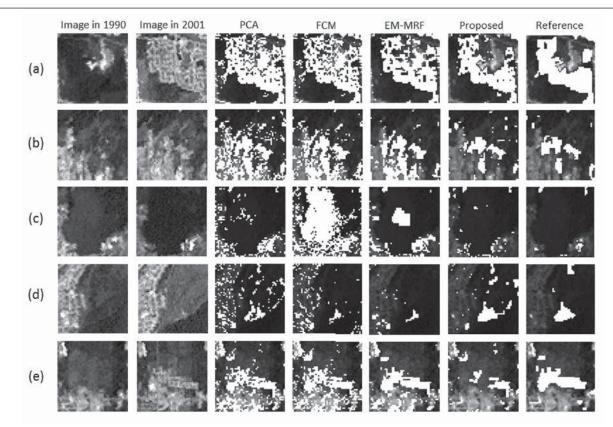
Figure 4. The subsets and change-detection results of four unsupervised for different subset scenes (The detected changes from different methods are shown in pure white): (a) *vegetation<->built-up area*; (b) *local reflectance change and vegetation<->built-up area*; (c) unchanged *water body with different quality*; and (d) *water<->barren land*; (e) *barren land<->built-up area*

mixed pattern (Ghosh *et al.*, 2011). It tries to find the best label for every pixel based on a fuzzy measure to represent a degree of a pixel belonging to one class. The final classification result can be estimated when an objective error function is minimized.

3. Expectation Maximum-Markov Random Field (EM-MRF)

Following Bruzzone and Prieto's framework (2000), an EM-MRF framework is constructed. This method first characterizes the density function of changed and unchanged classes after EM clustering. The final change mask can be obtained when the general energy reaches the minimum based on MRFs modal. To minimize the energy term, we use the same ICM algorithm in our proposed procedure.

Plate 2 shows the change-detection maps from three previous methods and our proposed method over the whole interested area for qualitative comparison. It is clear that PCA and FCM, as context-insensitive methods, both caused a certain amount of salt-and-pepper noise; among the three methods, FCM performed the worst as it labeled an almost unchanged region of water as the change. EM-MRF and our method, as context-sensitive methods, could obtain similar results with a low noise level.

Figure 4 shows the examples of five subsets with different change types and the detection results from three unsupervised method and our proposed method. We crop five sub-images with representative area of 50*50 pixels for each from original images and different detection maps in Plate 2. From the result, our proposed method can generally outperform the other three methods over the different change types. Especially for the noisy type of *local reflectance change* and *water*

quality change, PCA, FCM, EM-MRF all easily over-detect falsely, while our proposed method can keep them out for the final results (Figure 4b and Figure 4c). The only exception among all the examples is the case of *barren land<->built-up area* (Figure 4e). This is because we think the transition of *built-up area* to *barren land* with extremely smooth surface usually fails to hold distinguishing change on our saturation level, as their materials are similar, which affects the performance.

Table 2 is the result of the quantitative evaluation for the detection results from four methods using Im and Jensen's (2005) evaluating framework. A total of 800 sample points were randomly created within the study area. The reference data are acquired from Google Earth™ with the help of expert interpretation and field survey. Each subset (or pixel) is first spatially matched with the corresponding high spatial resolution image. The change type included in each pixel is then checked by manual interpretation. Based on the reference data, 141 sample pixels are categorized into "changed" and 659 are labeled as "unchanged." To compare the change detection accuracy of four techniques, the error matrix and the corresponding overall accuracy and Kappa statistic as well as user's and producer's accuracy are calculated (Story and Congalton, 1986; Congalton, 1991). Table 2 lists the error matrix derived for each method. The overall accuracy and Kappa statistic for our proposed method are 95.1 percent and 83.3 percent, both are the highest among four methods. EM-MRF is ranked the second and FCM and PCA perform the poorest based on the overall accuracy. When we look at the accuracy for individual classes, the performance of our proposed method is also the best among four methods for both "change" and "no-change" classes. However, compared with the individual user's and producer's accuracy of "no-change" class, the accuracy of "change" class from our proposed method are much

TABLE 2. ERROR MATRIXES FOR CHANGE DETECTION RESULTS FROM PCA, FCM, EM-MRF AND THE PROPOSED METHOD

Classification data		Reference Data			
		Change	No change	Row total	User's (%)
PCA: Overall accuracy=83.8% Kappa statistic: 50.6%					
Map data	Change	100	41	141	70.9
	No change	89	570	659	86.5
	Column total	189	611	800	-
	Producer's (%)	52.9	93.3	-	-
FCM: Overall accuracy=82.0% Kappa statistic: 46.6%					
Map data	Change	98	43	141	69.5
	No change	101	558	659	84.7
	Column total	199	601	800	-
	Producer's (%)	49.2	85.6	-	-
EM-MRF: Overall accuracy=91.9% Kappa statistic: 73.1%					
Map data	Change	116	25	141	82.3
	No change	40	619	659	93.9
	Column total	156	644	800	-
	Producer's (%)	74.4	96.1	-	-
Proposed: Overall accuracy=95.1% Kappa statistic: 83.3%					
Map data	Change	122	19	141	86.5
	No change	20	639	659	97.0
	Column total	142	658	800	-
	Producer's (%)	85.9	97.1	-	-

higher than the corresponding individual accuracy of PCA, FCM, and EM-MRF. The better performance of our proposed method clearly indicates the benefit of the complementary feature selection in our proposed method for urban change detection.

Discussion and Conclusions

This paper addresses the detection of land-cover change from the bi-temporal remote-sensing images. The proposed procedure mainly uses information from a very novel group of observations: luminance and saturation. Their nature for identifying different types of change occurred in urban area has been exploited; a procedure based on combining the two features is created by integrating automatic radiometric normalization, T-point thresholding, Bayes Fusion and Markov Random Field. For overall accuracy assessment, the proposed procedure is superior over three earlier referenced unsupervised methods.

The key component for our proposed model is feature design. We think the best feature number should be two since more features would greatly increase computation for MRFs modeling (e.g., three features will produce 27 initial classes for implementing MRFs). An efficient procedure for designing features should include the consideration of both (a) feature independence, and (b) separability of our change of interest from multiple changes. Since our features are derived from HSL color modal, their independence can be guaranteed for the subsequent Bayes classifier fusion; both visual and quantitative tests in our paper have indicated their perfect complementary nature for identifying only change of interest while keeping noisy types excluded.

Luminance feature is mainly contaminated by *low reflectance* to *high reflectance (LR->HR)*, which mostly occurs for the built-up area, such as the example of 'A' region in Plate 1a and Figure 4b. This can be explained by the fact that human activities often modify the surface of the built-up area (such as roof or road renovation), which results in reflectance change. Saturation feature easily results in false inclusion of inter-class changes of vegetation (*IC*) and water quality change (*QC*) as these two noisy changes mainly modify the color information of the land surface and slightly affect the reflectance level. Generally, saturation is less affected by local-reflectance changes since such changes are considered to exert roughly equivalent influences on three bands.

The results from the experiments indicate that the proposed procedure offers measureable advantages over the earlier unsupervised change detection (Plate 2 and Figure 4). The traditional techniques, such as FCM and EM-MRF, select changed pixels based only on the "measureable distances" to the center of changed and unchanged class, without any step for feature selection. This would lead to some errors. For example, if change is determined based on spectral bands (such as Red, Green, and Blue band), the noisy change of varied local illumination would exert changed magnitude for all the feature bands. As a result, some unchanged land-cover has a high variance of pixel values with large distances to the center of general unchanged class in the feature space, and thus is easy to be falsely classified as change class. Although PCA transform can be thought of as a method based on feature selection (the second component is chosen), it is not efficient since there is only one feature used for change detection.

It is noteworthy that the task of feature selection is problem-dependent, and heavily relies on the knowledge of the application domain. The proposed method is only tested for urban change-detection; for other applications such as forest damage or wetland monitoring, the complementary nature of lightness and saturation cannot be guaranteed since "real change" and "noisy change" need to be redefined. For future research, the exploitation of more change features and introduction of supervised frameworks remains to meet a variety of application scenes.

Acknowledgments

References

Benedek, C., and T Sziranyi, 2009. Change detection in optical aerial images by a multilayer conditional mixed Markov model, *IEEE Transactions on Geoscience and Remote Sensing*, 47(10):3416–3430.

Bruzzone, L., and D.F. Prieto, 2000. Automatic analysis of the difference image for unsupervised change detection, *IEEE Transactions on Geoscience and Remote Sensing*, 38(3):1171–1182.

Bruzzone, L., and D.F. Prieto, 2002. An adaptive semiparametric and context-based approach to unsupervised change detection in multitemporal remote-sensing images, *IEEE Transactions on Image Processing*, 11(4):452–466.

Chen, D., and S, Ye, 2015. Comparison of threshold selection methods for change detection from remotely sensed images, *Journal of Applied Remote Sensing*, (In review).

Cheng, H.-D., X. Jiang, Y. Sun, and J. Wang, 2001. Color image segmentation: Advances and prospects, *Pattern Recognition*, 34(12):2259–2281.

Coppin, P., I. Jonckheere, K. Nackaerts, B. Muys, and E. Lambin, 2004. Review Article: Digital change detection methods in ecosystem monitoring: A review, *International Journal of Remote Sensing*, 25(9):1565–1596.

Congalton, R.G., 1991. A review of assessing the accuracy of classifications of remotely sensed data, *Remote Sensing of Environment*, 37(1):35–46.

Coudray, N., J.-L.Buessler, and J.-P. Urban, 2010. Robust threshold estimation for images with unimodal histograms, *Pattern Recognition Letters*, 31(9):1010–1019.

Deng, J., K. Wang, Y. Deng, and G. Qi, 2008. PCA-based land-use change detection and analysis using multitemporal and multisensor satellite data, *International Journal of Remote Sensing*, 29(16):4823–4838.

Dhandra, B., R. Hegadi, M. Hangarge, and V. Malemath, 2006. Analysis of abnormality in endoscopic images using combined hsi color space and watershed segmentation, *Proceedings of the 18th International Conference on Pattern Recognition*, 2006, ICPR 2006.

Du, P., S. Liu, P. Gamba, K. Tan, and J. Xia, 2012. Fusion of difference images for change detection over urban areas, *IEEE Journal of Selected Topics in Applied Earth Observations and Remote Sensing*, 5(4):1076–1086.

Fernandez-Prieto, D., and M. Marconcini, 2011. A novel partially supervised approach to targeted change detection, *IEEE Transactions on Geoscience and Remote Sensing*, 49(12):5016–5038.

Ghosh, A., N.S. Mishra, and S. Ghosh, 2011. Fuzzy clustering algorithms for unsupervised change detection in remote sensing images, *Information Sciences*, 181(4):699–715.

Ghosh, S., N.S. Mishra, and A. Ghosh, 2009. Unsupervised change detection of remotely sensed images using fuzzy clustering, *Proceedings of the Seventh International Conference on Advances in Pattern Recognition, 2009*, ICAPR'09.Gillespie, A.R., A.B. Kahle, and R.E. Walker, 1986. Color enhancement of highly correlated images: I. Decorrelation and HSI contrast stretches, *Remote Sensing of Environment*, 20(3):209–235.

Grant, R., R. Green, and A. Clark, 2008. HLS Distorted colour model for enhanced colour image segmentation, *Proceedings of the 23rd International Conference on Image and Vision Computing New Zealand, 2008*, IVCNZ 2008.

Hu, X., C.V. Tao, and B. Prenzel, 2005. Automatic segmentation of high-resolution satellite imagery by integrating texture, intensity, and color features, *Photogrammetric Engineering & Remote Sensing*, 71(12):1399–1406.

Hussain, M., D. Chen, A. Cheng, H. Wei, and D. Stanley, 2013. Change detection from remotely sensed images: From pixel-based to object-based approaches, *ISPRS Journal of Photogrammetry & Remote Sensing*, 80:91–106.

Im, J., and J.R. Jensen, 2005. A change detection model based on neighborhood correlation image analysis and decision tree classification, *Remote Sensing of Environment*, 99(3):326–340.

Kasetkasem, T., and P.K. Varshney, 2002. An image change detection algorithm based on Markov random field models, *IEEE Transactions on Geoscience and Remote Sensing*, 40(8):1815–1823.

Kittler, J., M. Hatef, R.P. Duin, and J. Matas, 1998. On combining classifiers, *IEEE Transactions on Pattern Analysis and Machine Intelligence*, 20(3):226–239.

Kuncheva, L.I.,2004. *Combining Pattern Classifiers: Methods And Algorithms*, John Wiley & Sons.

Le Hégarat-Mascle, S., and R. Seltz, 2004. Automatic change detection by evidential fusion of change indices, *Remote Sensing of Environment*, 91(3):390–404.

Lei, Q. (1999). *Application of Landsat TM and Modular Airborne Imaging Spectrometer (MAIS) Data for Geological Investigations and Mineral Prospection in the Area of Shibaocheng-Changma, Province Gansu, China*, München, Utz.

Li, L., and M.K. Leung, 2002. Integrating intensity and texture differences for robust change detection, *IEEE Transactions on Image Processing*, 11(2):105–112.

Li, S., B. Zhang, D. Chen, L. Gao, and M. Peng, 2011. Adaptive support vector machine and Markov random field model for classifying hyperspectral imagery, *Journal of Applied Remote Sensing*, 5(1):053538–053511.

Lu, D., P. Mausel, E. Brondizio, and E. Moran, 2004. Change detection techniques, *International Journal of Remote Sensing*, 25(12):2365–2401.

Rogan, J., and D. Chen, 2004. Remote sensing technology for mapping and monitoring land-cover and land-use change, *Progress in Planning*, 61(4):301–325.

Rogerson, P.A. (2002). Change detection thresholds for remotely sensed images, *Journal of Geographical Systems*, 4(1):85–97.

Singh, A., 1989. Review article digital change detection techniques using remotely-sensed data, *International Journal of Remote Sensing*, 10(6):989–1003.

Sohl, T.L., 1999. Change analysis in the United Arab Emirates: An investigation of techniques, *Photogrammetric Engineering & Remote Sensing*, 65(4):475–484.

Story, M. and R.G. Congalton, 1986. Accuracy assessment: A user's perspective, *Photogrammetric Engineering & Remote Sensing*, 52(3):397–399.

Tomowski, D., S. Klonus, M. Ehlers, U. Michel, and P. Reinartz, 2010. Change visualization through a texture-based analysis approach for disaster applications, *Proceedings of the ISPRS TC VII Symposium*, 05-07 July, Vienna, Austria, *International Archives of Photogrammetry and Remote Sensing*, Vol. XXXIII, Part 7A.

Yang, X., and C. Lo, 2000. Relative radiometric normalization performance for change detection from multi-date satellite images, *Photogrammetric Engineering & Remote Sensing*, 66(8):967–980.

Zhang, C., and P. Wang, 2000. A new method of color image segmentation based on intensity and hue clustering, *Proceedings of the 15th International Conference on Pattern Recognition 2000*.

Zhang, L., M. Liao, L. Yang, and H. Lin, 2007. Remote sensing change detection based on canonical correlation analysis and contextual Bayes decision, *Photogrammetric Engineering & Remote Sensing*, 73(3):311–318.